

## THE INFLUENCE OF CALCINATION TEMPERATURE ON IRON OXIDE ( $\alpha$ -Fe<sub>2</sub>O<sub>3</sub>) TOWARDS CO<sub>2</sub> ADSORPTION PREPARED BY SIMPLE MIXING METHOD

(Kesan Suhu Pengkalsinan Ferum Oksida ( $\alpha$ -Fe<sub>2</sub>O<sub>3</sub>) Disediakan Melalui Kaedah Campuran Ringkas Terhadap Penjerapan CO<sub>2</sub>)

Azizul Hakim<sup>1\*</sup>, Mohd. Ambar Yarmo<sup>1</sup>, Tengku Sharifah Marliza<sup>1,2</sup>, Maratun Najiha Abu Tahari<sup>1</sup>, Wan Zurina Samad<sup>1</sup>, Muhammad Rahimi Yusop<sup>1</sup>, Mohamed Wahab Mohamed Hisham<sup>1</sup>, Norliza Dzakarria<sup>1,3</sup>

<sup>1</sup>Catalysis Research Group, School of Chemical Sciences and Food Technology, Faculty of Science and Technology, Universiti Kebangsaan Malaysia, 43600 UKM Bangi, Selangor, Malaysia

<sup>2</sup>Catalysis Science and Technology Research Centre, Faculty of Science, Universiti Putra Malaysia, 43400 UPM Serdang, Selangor, Malaysia

<sup>3</sup>School of Chemistry and Environmental, Faculty of Applied Science, University Teknologi Mara (UiTM) Negeri Sembilan, Kampus Kuala Pilah, Pekan Parit Tinggi, 72000 Kuala Pilah, Negeri Sembilan, Malaysia

\*Corresponding author: [azizulhakim2442@gmail.com](mailto:azizulhakim2442@gmail.com)

Received: 7 February 2016; Accepted: 3 July 2016

### Abstract

Synthesized iron oxide,  $\alpha$ -Fe<sub>2</sub>O<sub>3</sub> used for CO<sub>2</sub> capturing was prepared by a simple mixing method and calcined at temperatures in a range of 350 – 850 °C. CO<sub>2</sub> adsorption isotherms at 25 °C and 1 atm found that the sample namely s450 that calcined at 450 °C gave the highest CO<sub>2</sub> adsorption activity with the adsorption capacity of 17.0 mg<sub>CO2</sub>/g<sub>adsorbent</sub>. Monodentate carbonate, bidentate carbonate and bicarbonates formation were observed on s450 through the IR spectra. The basicity of s450 was identified by chemisorption of CO-TPD which contains weak, medium and strong basic sites with CO total adsorbed amount of 1.99 cm<sup>3</sup>/g. It was found that s450 calcined at 450 °C has certain crystallite peaks that abruptly increased through the XRD diffractogram. The texture properties of s450 generated high porosity and more uniform sphere shape particle size with high surface area (50.5 m<sup>2</sup>/g). Furthermore, it is composed of trimodal distribution for pore size distribution curve desirable for CO<sub>2</sub> adsorption.

**Keywords:** CO<sub>2</sub> capture, adsorption, iron oxide, solid adsorbent, porosity

### Abstrak

Penjerapan CO<sub>2</sub> terhadap ferum oksida,  $\alpha$ -Fe<sub>2</sub>O<sub>3</sub> yang disintesis melalui kaedah campuran ringkas dan dikalsin pada suhu 350-850 °C. Penjerapan isoterma CO<sub>2</sub> pada suhu bilik, 25 °C and 1 atm mendapati sampel s450 yang dikalsin pada suhu 450 °C menunjukkan aktiviti penjerapan CO<sub>2</sub> paling tinggi dengan keupayaan penjerapan sebanyak 17.0 mg<sub>CO2</sub>/g<sub>penjerap</sub>. Spektrum IR telah membuktikan pembentukan spesis monodentat karbonat, bidentat karbonat dan bikarbonat pada s450. Sifat bes s450 yang dikenalpasti menggunakan jerapan kimia CO-TPD dimana jumlah CO yang dijerap oleh tapak bes lemah, sederhana dan kuat adalah 1.99 cm<sup>3</sup>/g. Difraktogram XRD pula menunjukkan terdapat beberapa puncak kekisi yang meningkat. Tekstur s450 pula mempunyai keporosan yang tinggi dan bentuk sfera yang lebih sekata serta luas permukaan yang tinggi (50.5 m<sup>2</sup>/g). Tambahan lagi, graf taburan saiz liang s450 juga terdiri daripada taburan jenis trimodal yang menjadi salah satu faktor penting dalam penjerapan CO<sub>2</sub>.

**Kata kunci:** penjerapan CO<sub>2</sub>, penjerapan, ferum oksida, penjerapan pepejal, keporosan

### Introduction

The main concern worldwide over the recent years is renewable energy which could generate for the rest of decades without worrying about the depletion of sources in the earth. Human population and consumption are directly proportional with the addition of technology provided and yet keep growth explosively which completed with extensive research and development in the industry and academic. This progressive situation made human realized with considerable attentions were paid to the green technology by using the anthropocentric environmental ethics which is people centered as an approach to reduce environmental pollutions and save the earth and future generation. It gave rise to anthropocentric individuals to feel the environment should be protected because of its value in maintaining or enhancing the quality of life for human [1].

Rapid growth development resulting in harmful air pollutants released into the atmosphere which became the major contribution in the global warming and several issues on urban smog, acid rain, and health problems contributed from emission of anthropogenic CO<sub>2</sub> [2]. The CO<sub>2</sub> in atmosphere, one of the major greenhouse gases, is now higher than the safety limit for the atmospheric CO<sub>2</sub> level of 350 ppm. According to the National Oceanic and Atmospheric Administration (NOAA) in U.S, the CO<sub>2</sub> level was higher than the safety limit since 80's and to date on September 2015 was approximately 397.63 ppm. Furthermore, the increased CO<sub>2</sub> growth rate about 2.0 ppm/year gives rise to the mitigating measure of capturing CO<sub>2</sub> [3].

According to Freund and Roberts [4], chemisorbed species is connected with the formation of CO<sub>2</sub><sup>δ-</sup>, the anionic molecule, which involves the charge transfer from the metal to the molecule. Consequently, the  $\alpha$ -Fe<sub>2</sub>O<sub>3</sub> decorated as the basic oxide where the CO<sub>2</sub> chemisorption involves the basic sites that act as electron donors and are associated with O<sub>2</sub><sup>-</sup> ions localized on surface defects [5]. The physisorption is found in almost all cases whereas the chemisorbed species are only observed under very specific conditions: the surfaces have to be either atomically rough, containing a high defect density in order to stabilize the chemisorbed species, or are alkali metal modified surfaces [4].

Metal oxides of calcium oxide (CaO) were among the earliest studies in the CO<sub>2</sub> capture that has promising properties of high adsorption capacity [6]. However, it consumed high energy during the desorption process up to 900 °C which is economically not favourable. Thus, the capability of the alternative adsorbents from the metal oxides was studied. The desorption process that required heat to dissociate formed carbonate can be explained by the interaction of CO<sub>2</sub> as adsorbate on the adsorbent which depends on its binding energy. In fact, others than alkali metal and alkali earth metal oxides, several metal oxides have been reported for a single crystal oxide that shows its capability in the CO<sub>2</sub> capture. Kwon et al. [7] reported the dissociation carbonate product on lanthanum sesquioxide (La<sub>2</sub>O<sub>3</sub>) using the IR frequencies at 500°C. Furthermore, the desorption temperature was increased to 700 °C when higher pressure was used during the CO<sub>2</sub> adsorption [8]. Silver oxide (AgO) exhibited desorption temperature at 247°C that was observed under the scanning tunnelling microscopy (STM) [9]. Meanwhile, Yoshikawa [10] discovered the order of dissociation of the different carbonate species (bicarbonate, monodentate, bidentate and polydentate carbonate) on cerium oxide (CeO<sub>2</sub>) at the temperature range of 50 – 450 °C. Among the copper oxides (CuO and Cu<sub>2</sub>O), it was found that copper (II) oxide (CuO) showed a higher adsorption capacity by physisorbed of 17.7 mg CO<sub>2</sub>/g adsorbent and chemisorbed of 9.5 mmol/g with three times regeneration without significant loss of performance [11]. Our works reported that NiO exhibited adsorption capacity of 14.1 and 87.0 mg CO<sub>2</sub>/g adsorbent by physio- and chemisorption respectively, with the desorption temperature range of 400 – 460 °C [12].

Previous studies of iron oxides,  $\alpha$ -Fe<sub>2</sub>O<sub>3</sub> as adsorbent showed evidence on the presence of various carbonate species formations such as monodentate, bidentate, and bicarbonate forms on the metal oxides adsorbent surface [13-17]. These studies described carbonates formation using the Fourier transfer infra red (FTIR) spectroscopy to analyze the configuration of C-O interaction with iron oxide surface. Ismail et al. [18] reported CO<sub>2</sub> adsorption by using the iron material from a steel-pickling waste (97 wt% FeSO<sub>4</sub>·7H<sub>2</sub>O). The original material was roasted at 700 °C for 5 hours in air, oxygen, and nitrogen prior to the adsorption process. However, none of these researches reported the basicity active site that contributes to CO<sub>2</sub>.

In this study,  $\alpha$ -Fe<sub>2</sub>O<sub>3</sub> was synthesized by using a simple mixing method in order to obtain the preferable surfaces. The  $\alpha$ -Fe<sub>2</sub>O<sub>3</sub> was synthesized by using a low cost method to identify the optimum calcination temperature and quantify the basicity properties. Hence, the amount of CO<sub>2</sub> adsorbed physically at room temperature, 25°C and 1 atm was measured using the volumetric adsorption technique.

## Materials and Methods

### Sample preparation

The analytical grade iron (III) nitrate nonahydrate (Fe(NO<sub>3</sub>)<sub>3</sub>·9H<sub>2</sub>O, 98%) and ethanol (C<sub>2</sub>H<sub>5</sub>OH, 99.7%) were purchased from Sigma-Aldrich, USA and System, Malaysia respectively. The bulk  $\alpha$ -Fe<sub>2</sub>O<sub>3</sub> obtained from BDH, United Kingdom was treated by calcined under nitrogen flow at 150 °C for 1 hour. The simple mixing method is very useful to produce  $\alpha$ -Fe<sub>2</sub>O<sub>3</sub> nanoparticles with low cost of starting materials. This method was modified from literature reported by Dong et al. [19]. The Fe(NO<sub>3</sub>)<sub>3</sub>·9H<sub>2</sub>O was weighed to 16.16 g and dissolved in 20 ml distilled water to have concentration of 2 M. To this solution, ethanol was added with a volume percentage of 25% from the distilled water used and stirred for 1 hour at room temperature. The concentration of 2 M precursor was found to be the shortest time formation with a connection of large number of Fe(OH)<sub>3</sub> fine particles. Ethanol acts as a stabilizer for the colloidal particles avoid aggregation [19]. The solution was sonicated for 20 minutes to obtain better homogeneous condition and dried with vigorous stirring at the temperature of 80 – 100 °C. The dried solid was ground and kept in an oven for 24 hours at 110 °C. Finally, it was calcined under the air flow at the temperature ranging from 350 – 850 °C. The samples were labeled by the calcination temperatures namely: bulk, s350, s450, s550, s650, s750 and s850.

### Characterization

These samples were characterized with Bruker AXS D8 Advance type with X-ray radiation source of Cu K $\alpha$  (40 kV, 40 mA) to obtain the X-ray Diffraction (XRD) pattern. The crystal structures were verified by recording 2 $\theta$  diffraction angle from 10° to 90° at wavelength ( $\lambda$  = 0.154 nm). The diffraction pattern obtained was matched with a standard diffraction data (JCPDS) file for identification of the crystalline phase composition.

The physical surface analysis of N<sub>2</sub> adsorption-desorption was conducted at 77 K in a Micromeritics ASAP 2020 instrument to determine the textural surface properties of the prepared samples. The catalysts were degassed at 200°C for 6 hours prior to analysis. The volumetric adsorption apparatus was used to determine the surface area and N<sub>2</sub> adsorption-desorption isotherm using the BET equation [20]. Pore volumes and pore size distribution were determined by Barret–Joyner–Halenda (BJH) method and applied based on the adsorption branch. The *t*-plot method was used to calculate the non-microporous (or external) surface area considerable as the mesoporous surface area [21-23]. The total pore volumes were estimated to be the liquid volume of adsorbate (N<sub>2</sub>) at a relative pressure. All surface areas were calculated from the N<sub>2</sub> adsorption isotherms by assuming the area of a N<sub>2</sub> molecule to be 0.162 nm<sup>2</sup> [20]. The CO<sub>2</sub> adsorption behaviors of the sorbents were evaluated using the above mentioned instrument and evaluated at 25°C and 1 atm with circulated water bath and using 99.9% of purified CO<sub>2</sub> gas as adsorbate.

The particle sizes and morphology of the catalysts were measured by the transmission electron microscopy (TEM, CM12 Philips) which is equipped with an electron gun 200 kV. The synthesized of  $\alpha$ -Fe<sub>2</sub>O<sub>3</sub> before and after the exposure with CO<sub>2</sub> (5% and 15% of CO<sub>2</sub>) as well as after temperature programmed desorption (TPD) at 650°C were examined using the Fourier transform infrared (FTIR) spectroscopy. The spectra of the samples were recorded between 4000 and 650 cm<sup>-1</sup> in spectrum 400, FTIR Spectrometer (Perkin Elmer, UK) using the Attenuated Total Reflection (ATR) method for the sample preparation technique.

The basicity properties of catalysts were performed by the TPD from a conventional apparatus of Chemisorption Analyzer, Micrometrics 2920 Chemisorb. This instrument is equipped with a thermal conductivity detector (TCD). Approximately 50 mg of catalyst was preheated to 150°C to remove the moisture for 30 minutes before it was cooled down to 30°C under the pure He gas flow rate of 30 mL/min. The catalyst was exposed with a gas mixture of 5% CO in He in a constant temperature of 40°C under flow rate 30 mL/min for 60 minutes. The pure He gas again was introduced to the catalyst for the purpose of removing excess of the weak physically adsorbed CO at 50°C for 30 minutes. The TPD required ice to trap the moisture which was placed in the container of instrument prior to the

measurements and heated to  $900^\circ\text{C}$  with the heating rate of  $10^\circ\text{C}/\text{min}$  under pure He. The samples after the  $\text{CO}_2$ -TPD analysis by using 5% and 15%  $\text{CO}_2$  were collected using above mentioned conditions and observed through FTIR.

## Results and Discussion

### XRD Pattern

The X-ray diffractograms of bulk and synthesized  $\alpha\text{-Fe}_2\text{O}_3$  were determined and are represented in Figure 1. The peaks observed at d-values of 3.68, 2.70, 2.52, 2.20, 1.84, 1.69, 1.60, 1.49, 1.45, 1.34, 1.31, 1.26, 1.22, 1.19, 1.16, 1.14,  $1.10 \text{ \AA}$  in all catalysts correspond to the rhombohedral phase of hematite,  $\alpha\text{-Fe}_2\text{O}_3$  with lattice parameters  $a=5.0356$  and  $c=13.7489$  (matched with JCPDS number 33-0664). The diffractograms show that the crystal formation of hematite phases can be seen at the calcination temperature of  $350^\circ\text{C}$ . Nevertheless, the crystallite peaks appear at this temperature had lower intensity compared to the bulk hematite especially on crystallites (018), (208), (10 10), (220), (306), (128), (02 10), (134) and (226). The s450 was found to have a better crystallinity of synthesized  $\alpha\text{-Fe}_2\text{O}_3$  among others. The crystallite peaks of (024), (116), (214) and (300) were abruptly increased for the calcined  $\alpha\text{-Fe}_2\text{O}_3$  at  $450^\circ\text{C}$ . The XRD pattern for the calcination temperatures ranging at  $550 - 850^\circ\text{C}$  had similar intense of crystallinity.

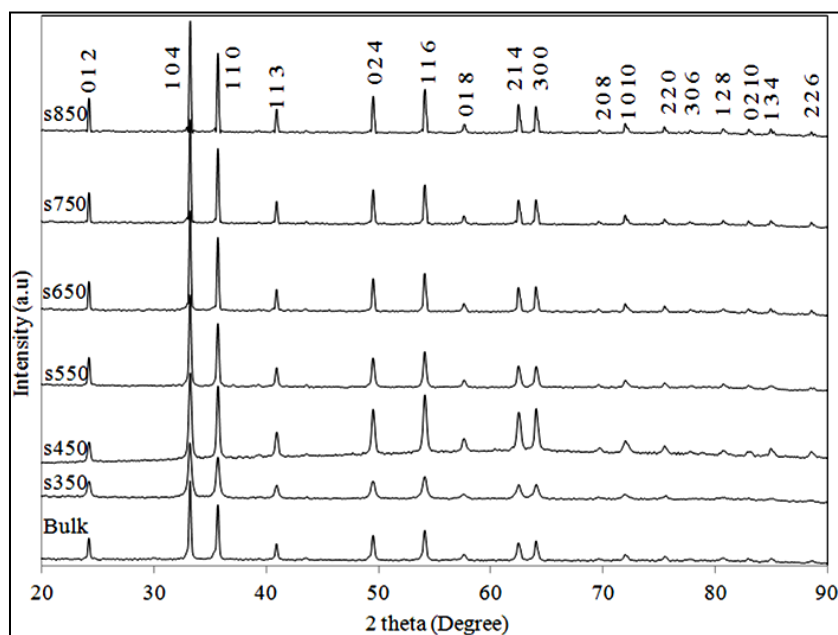


Figure 1. XRD patterns of  $\alpha\text{-Fe}_2\text{O}_3$  at different calcination temperatures

### Textural properties

The  $\text{N}_2$  adsorption-desorption isotherms, specific surface areas, and pore volumes for the bulk and synthesized  $\alpha\text{-Fe}_2\text{O}_3$  are presented in Figure 2 and Table 1, respectively. The isotherms for all samples are type III profile according to the IUPAC isotherms of classification with typical sloping adsorption and desorption branches covering a large range of relative pressure ( $P/P_0$ ) where the adsorbent-adsorbate interaction is weak, but could be obtained with certain porous adsorbents [24]. It was proven from the H3 type hysteresis based on the isotherms ascribed from plate-like particles giving rise to slit-shaped pores from the adsorbent. The adsorbents showed large ranges of pore diameters which do not exhibit any limiting adsorption at high  $P/P_0$  [20]. The adsorbents consist of mesoporous and macroporous structure in all samples based on the isotherms. It is interesting to note that s450 has the largest hysteresis area (Figure 2) compared to others which indicate the highest mesoporous and macroporous structure on the surface. The mesopore surface area with pore size ranging between 2 to 50 nm was evaluated by the

t-plot method. The macropore structure of bulk  $\alpha$ -Fe<sub>2</sub>O<sub>3</sub> was contributed more than mesopore since the mesopore surface area was smaller (3.9 m<sup>2</sup>/g) than s650 (4.2 m<sup>2</sup>/g) (Table 1). For s350, the temperature of 350 °C was not enough to create better pore structure. However, the sample s450 calcined at 450 °C created better pore structure which leads to a high surface area (50.5 m<sup>2</sup>/g). Hence, the total pore volume was increased which is desirable for the adsorption behavior. This ascribed to the calcined  $\alpha$ -Fe<sub>2</sub>O<sub>3</sub> at a particular temperature provided the capability in generating well pore structure nor produced fine particles. At the temperature higher than 450 °C, it was found to be not efficient to obtain a high porosity  $\alpha$ -Fe<sub>2</sub>O<sub>3</sub>. The constituent crystallites of the hematite grew and sintered resulting from the increased of thermal exposure, eventually generated smaller pores and also reduced the BET surface area. The low specific surface area indicative of less-defined porosity was observed for s550 and above. The bulk  $\alpha$ -Fe<sub>2</sub>O<sub>3</sub> exhibited better adsorption rather than s650 and above.

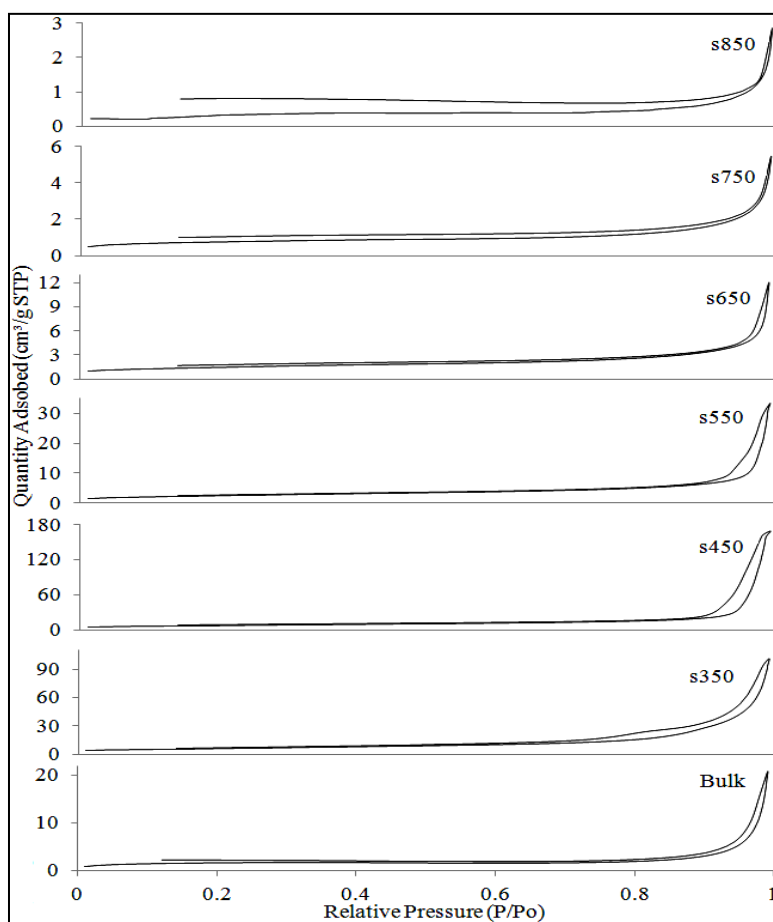


Figure 2. The effect of calcination temperature on  $\alpha$ -Fe<sub>2</sub>O<sub>3</sub> towards N<sub>2</sub> adsorption-desorption isotherms

### Pore size distribution

The highest N<sub>2</sub> adsorption with the widest range of pore size can be seen from the pore size distribution curve illustrated in Figure 3. The distribution shows a wide range of pore sizes categorized under mesoporous and macroporous. A trimodal distribution was observed clearly for  $\alpha$ -Fe<sub>2</sub>O<sub>3</sub> calcined at 450 °C whereas the rest adsorbents established similar distribution and several multimodal distributions. The trimodal distribution has overcome the monomodal which appears to produce an enhancement in the surface area of the synthesized metal oxides [25]. It is interesting to note that s450 has three maximum pore diameter (652, 907 and 1271 Å) located in a

wide pore structure. These pores exhibited narrow pore size distribution compared to the others which are indicative of good porosity for gas adsorption retained based on the pore size distribution and BET surface area obtained.

Table 1. Textural parameters of the samples obtained from the N<sub>2</sub> adsorption-desorption and CO<sub>2</sub> adsorption isotherms

Calcination Temperature (°C)	BET Surface area (m <sup>2</sup> /g)	Mesopore Surface area (m <sup>2</sup> /g)	Total Pore volume (cm <sup>3</sup> /g)	Pore diameter (Å)	CO <sub>2</sub> Adsorption at 25 °C (cm <sup>3</sup> /g)	Adsorption Capacity at 25 °C (mg CO <sub>2</sub> /g <sub>adsorbent</sub> )
Bulk	5.7	3.9	0.022	154	1.53	3.0
s350	23.1	20.6	0.124	215	2.91	5.7
s450	50.5	27.0	0.227	371	8.66	17.0
s550	9.3	8.9	0.039	168	1.17	2.3
s650	5.0	4.2	0.012	96	1.11	2.2
s750	2.6	1.7	0.006	91	0.94	1.8
s850	1.2	1.9	0.003	98	0.76	1.5

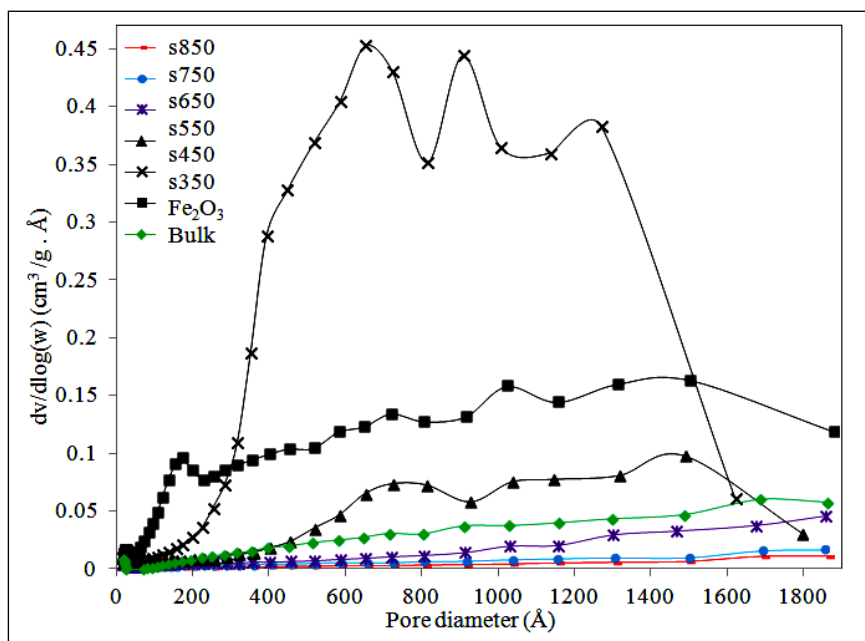


Figure 3. Pore size distribution of synthesized  $\alpha$ -Fe<sub>2</sub>O<sub>3</sub> by BJH method

#### Pore structure of the adsorbents

The bright field TEM micrographs of  $\alpha$ -Fe<sub>2</sub>O<sub>3</sub> prepared with increased calcination temperature are illustrated in Figure 4 to observe its crystallographic and morphological structure. The bulk  $\alpha$ -Fe<sub>2</sub>O<sub>3</sub> has larger crystallite size particles at 160.5 nm with aggregation and less pore structure which has agreement with the mesopore surface area based on N<sub>2</sub> adsorption-desorption isotherms. For s350, it did not show very good morphology and aggregation of

the particles with particle size range 12.6 to 57.0 nm. Nonetheless, small and uniform particle sizes of  $\alpha\text{-Fe}_2\text{O}_3$  particles with range of 24.5 to 56.0 nm were generated for s450. The pore structures well distributed on the particles surface are also easily seen from Figure 4. The one-hour calcination temperature of 550 °C was enough to make the particle size of s550 became larger (44.2 to 90.3 nm). At 650 °C, s650 exhibited more particles changing to ellipsoid with larger particle range of 73.0 to 119.2 nm and fine pore structure was observed. According to Dong et al. [19], particles changed at a higher temperature of 700 °C for longer calcination time of three hours. The porous images in Figure 4 for synthesized  $\alpha\text{-Fe}_2\text{O}_3$  by using simple mixing method could provide improvement in the porosity rather than bulk sample. The high porosity surfaces provide more active sites and space which are responsible in attracting  $\text{CO}_2$ .

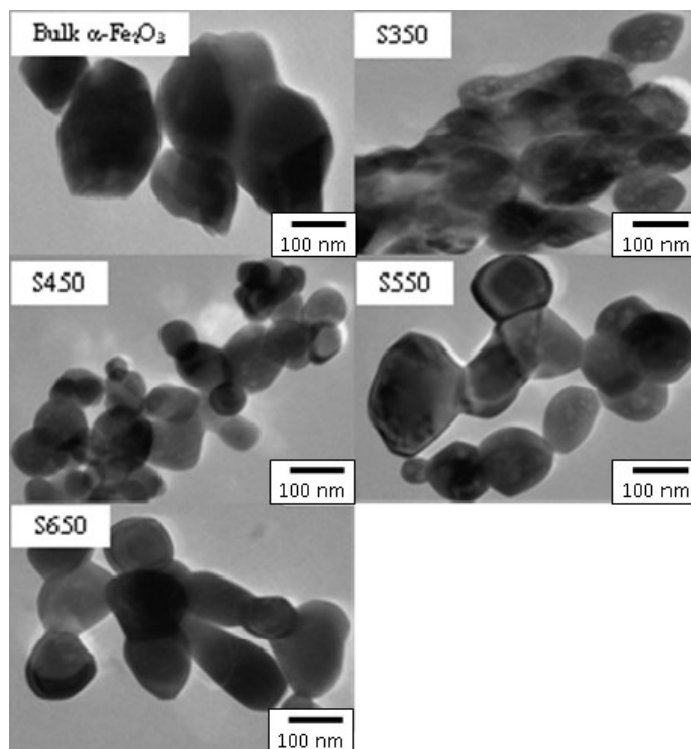


Figure 4. TEM view of synthesized  $\alpha\text{-Fe}_2\text{O}_3$  particles

#### Base strength distribution by CO-TPD analysis

The s450 was chosen based on the morphology studies, and used for the basicity measurement by TPD with CO as the probe molecule due to having the desirable properties in the  $\text{CO}_2$  adsorption. Although  $\text{CO}_2$  has been used worldwide for this purpose, somehow it could appear to be proper probe molecule because of its acidic in nature. The basic of adsorbent would attract the acidic gas easily to form various interaction modes. The CO-TPD profile in the literatures varies depending on the adsorption condition of CO. The broad desorption or high intensity peak indicative of CO has been adsorbed. The CO-TPD peaks represent the base strength distribution of the adsorbent are shown in Figure 5. The range of weak, medium and strong basic sites were estimated from the area under their TPD curve of 40 – 200, 200 – 400, >400 °C respectively. The temperature ranges chosen for the weak, medium and strong basic sites are CO-TPD observed from the most catalyst [26, 27]. The strengths of the basic sites are expressed in the temperature range wherein the  $\text{CO}_2$  chemisorbed on the basic sites was desorbed. The CO-TPD curve showed maximum temperature of 170 °C (weak base), 314 °C (medium base) and 641 °C (strong base) with the desorption quantity of 0.14, 0.42 and 1.43  $\text{cm}^3/\text{g}$  respectively. This adsorbent had total amount of 1.99  $\text{cm}^3/\text{g}$  resulting a potential adsorbent in  $\text{CO}_2$  adsorption.

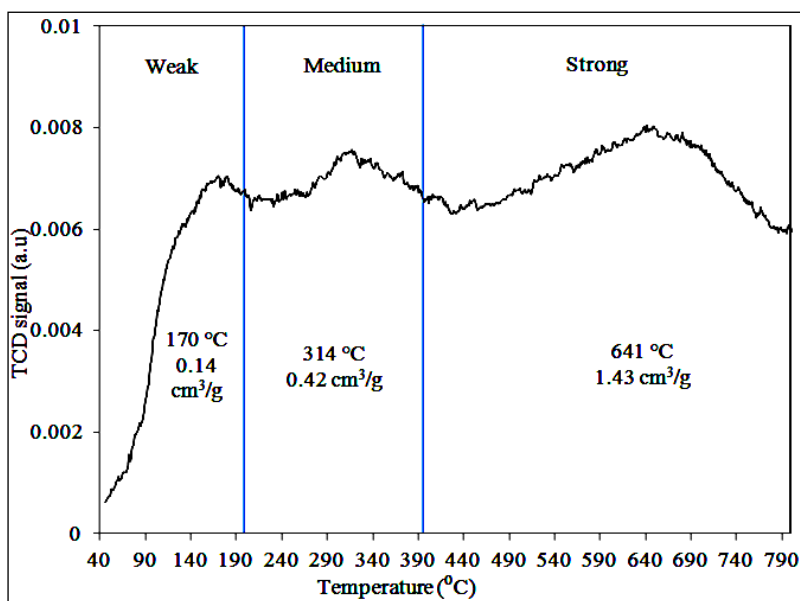


Figure 5. Base strength distribution from TPD profile of CO adsorption (CO-TPD) for s450

#### Formation of carbonate

The IR spectra for s450 obtained before and after being exposed to  $\text{CO}_2$ , and after desorption of  $\text{CO}_2$  are shown in Figure 6 and vibrational frequencies assignments are tabulated in Table 2. The position of the bands at  $1226$  and  $1630\text{ cm}^{-1}$  are indicative of the bicarbonate species for C-OH bending mode and asymmetry O-C-O vibrational modes of adsorbed bicarbonates respectively [15-17, 28]. The bicarbonate can be easily identified by its OH peak at  $3639\text{ cm}^{-1}$  [15-17, 28]. Other peaks observed at  $1038$  and  $1399\text{ cm}^{-1}$  were associated with the monodentate structures of carbonate from IR spectra with C-O stretches and symmetry O-C-O vibrational mode respectively [15-17]. The  $1399\text{ cm}^{-1}$  peak only appeared for  $\alpha\text{-Fe}_2\text{O}_3$  with 5%  $\text{CO}_2$  of exposure. The weak contributions around  $1245$  and  $1554\text{ cm}^{-1}$  agreed with the formation of surface bidentate carbonate species with symmetry (O-C-O) and asymmetry (O-C-O) stretching respectively [15-17, 29] as a consequence of the adsorption of  $\text{CO}_2$  on a metal oxide surface. In all spectra, the CO band from bridging  $\text{CO}_2$  at  $2035\text{ cm}^{-1}$  was more intense for  $\alpha\text{-Fe}_2\text{O}_3$  exposed with 15%  $\text{CO}_2$  [30]. The intensity pattern of peak  $2162\text{ cm}^{-1}$  was similar where C=O bonded with hydroxyl groups having weak acidic properties [31]. The broad IR absorption band at  $3370\text{ cm}^{-1}$  was the characteristic of H-O-H bonding of the  $\text{H}_2\text{O}$  molecules which shows the presence of hydroxyl groups [32]. The intensities of hydroxyl group were found to be reduced and partially removed after  $\text{CO}_2$ -TPD at  $650\text{ °C}$  due to the thermal exposure. Additionally, there was also a broad OH stretching region of  $2700$  to  $3706\text{ cm}^{-1}$  for all spectra but more intense for those exposed with 5% and 15%  $\text{CO}_2$  which was caused from moisture in the gas mixture. The adsorption band at  $918\text{ cm}^{-1}$  was corresponded to the Fe-O-H deformation due to the source of gas containing traces amount of moisture that led to the hydroxide compound formation on metal oxide surface [33, 34].



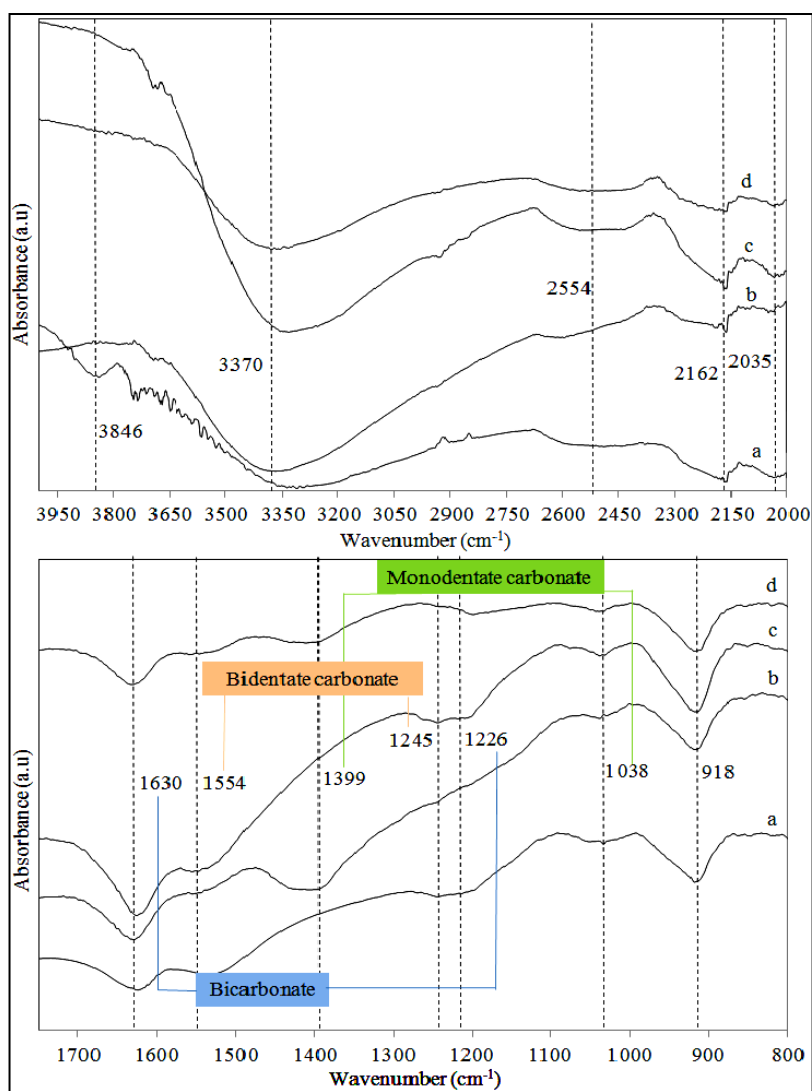


Figure 6. IR spectra of (a) s450 before CO<sub>2</sub> adsorption, (b)  $\alpha$ -Fe<sub>2</sub>O<sub>3</sub> at 450 °C exposed with 5% CO<sub>2</sub>, (c)  $\alpha$ -Fe<sub>2</sub>O<sub>3</sub> at 450 °C exposed with 15% CO<sub>2</sub> and (d)  $\alpha$ -Fe<sub>2</sub>O<sub>3</sub> at 450 °C after CO<sub>2</sub>-TPD at 650 °C

Table 2. Vibrational modes of IR spectroscopy for s450 adsorbed product after CO<sub>2</sub> adsorption and CO<sub>2</sub>-TPD at 650 °C

Vibrational Modes	Frequency (cm <sup>-1</sup> )	References* (cm <sup>-1</sup> )	References
Bicarbonate (HCO <sub>3</sub> <sup>-</sup> )			
Asymmetry O-C-O	1630	1555-1720	[15-17, 28]
C-OH	1226	1220-1269	[15-17, 28]
O-H	3639	3600-3627	[15-17, 28]

Table 2 (cont'd). Vibrational modes of IR spectroscopy for s450 adsorbed product after CO<sub>2</sub> adsorption and CO<sub>2</sub>-TPD at 650 °C

Vibrational Modes	Frequency (cm <sup>-1</sup> )	References* (cm <sup>-1</sup> )	References
Carbonate (CO <sub>3</sub> <sup>2-</sup> )			
Monodentate			
C-O	1038	1040	[15-17]
Symmetry O-C-O	1399	1380-1395	[15-17]
Bidentate			
Symmetry O-C-O	1245	1243-1355	[15-17, 29]
Asymmetry O-C-O	1554	1535-1670	[15-17, 29]
Bridging CO <sub>2</sub>	2035	2035	[30]
CO <sub>2</sub> bonded to O-H	2162	2160-2162	[31]
H-O-H	3370	3370	[32]
Fe-O-H	918	800-920	[33, 34]

#### CO<sub>2</sub> adsorption

CO<sub>2</sub> adsorption isotherms of the adsorbents at 25 °C and 1 atm are shown in Figure 7 and the adsorption capacity is tabulated in Table 1. The CO<sub>2</sub> adsorption branch began from the monolayer that was on the adsorbent surface and continued with the multilayer adsorptions that is known as physisorption. The bulk  $\alpha$ -Fe<sub>2</sub>O<sub>3</sub> shows the adsorption capacity was 1.53 cm<sup>3</sup>/g. For the synthesized  $\alpha$ -Fe<sub>2</sub>O<sub>3</sub>, the CO<sub>2</sub> adsorption capacity varies with the different calcination temperature parameters. s450 exhibited the highest BET surface area and total pore volume, showed the highest CO<sub>2</sub> adsorption capacity (17.0 mg<sub>CO2</sub> / g<sub>adsorbent</sub>) at 25 °C and 1 atm. The amounts of CO<sub>2</sub> adsorbed onto the synthesized  $\alpha$ -Fe<sub>2</sub>O<sub>3</sub> decreased progressively as the calcination temperature was increased which was influenced by poor surface area as a consequence of the sintering effect of the adsorbent. It also has a higher volume of narrower pores with trimodal distribution of the pore size as shown in Figure 3, that provides more spaces to capture CO<sub>2</sub>. The adsorption capacity for s350 was rather higher than the rest of temperatures ascribed to crystallite grew and not exposed to the high thermal treatment that lead to sintering. The adsorption capacity for bulk  $\alpha$ -Fe<sub>2</sub>O<sub>3</sub> which was treated at 150 °C under N<sub>2</sub> recorded a higher value than s550 and above. In addition, the adsorbed weights (CO<sub>2</sub>) of all the adsorbents are in the following order: 450 > 350 > bulk > 550 > 650 > 750 > 850. In fact, a linearly proportional relationship between the adsorptive capacity and surface area is suggested. Higher surface area provides more active sites to attract CO<sub>2</sub> which resulting in high adsorption capacity. Overall, the simple mixing method could save more energy on the calcination temperature compared to Ismail et al. [18] work which required 700°C for the CO<sub>2</sub> adsorption purpose.

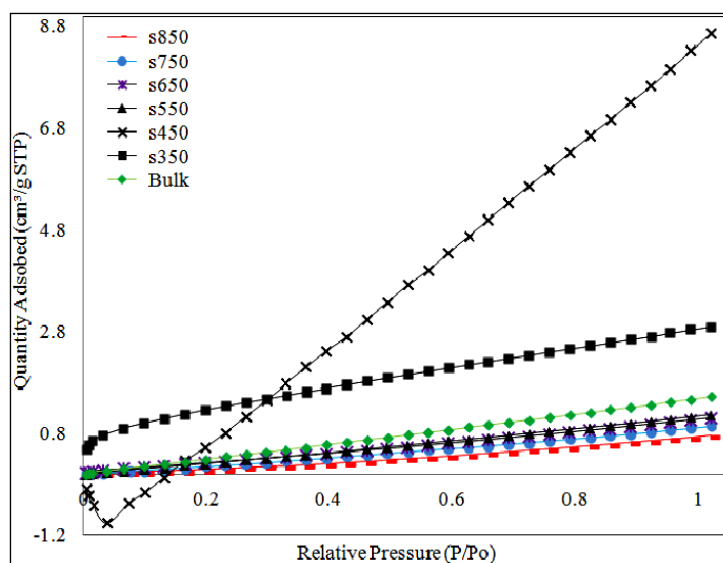


Figure 7. The effect of calcination temperatures on CO<sub>2</sub> adsorption isotherms at 25 °C and 1 atm

### Conclusion

The calcination temperature of  $\alpha$ -Fe<sub>2</sub>O<sub>3</sub> at 450 °C by using a simple mixing method generated sphere particle size of fine particles with high BET surface area, mesopore surface area, and total pore volumes. These features provide an enhancement in CO<sub>2</sub> adsorption at 25 °C and 1 atm with the highest adsorption capacity among all adsorbents was 17.0 mg<sub>CO2</sub>/g<sub>adsorbent</sub>. Furthermore, the total basic site presence for all three weak, medium and strong basic site was 1.99 cm<sup>3</sup>/g. The striking peak was observed at strong base site with amount of 1.43 cm<sup>3</sup>/g. The IR spectra described various configurations of CO<sub>2</sub> interacted with  $\alpha$ -Fe<sub>2</sub>O<sub>3</sub> surface by monodentate, bidentate and bicarbonate forms although exposed with low concentration of 5% of CO<sub>2</sub>.

### Acknowledgement

The authors wish to thanks Universiti Kebangsaan Malaysia (UKM) for funding this project under research grant number LRGS/BU/2011/USM-UKM/PG/02, BKBP-FST-K003323, ETP-2013-066 and TD-2014-024 from Ministry of Higher Education (MOHE) Malaysia and Centre of Research and Innovation Management (CRIM) UKM for the instruments facilities.

### References

1. Gagnon, S. C. and Barton, M. A. (1994). Ecocentric and anthropocentric attitudes toward the environment. *Journal of Environmental Psychology*, 14: 149 – 157.
2. Song, C. S. (2006). Global challenges and strategies for control, conversion and utilization of CO<sub>2</sub> for sustainable development involving energy, catalysis, adsorption and chemical processing. *Catalysis Today*, 115: 2 – 32.
3. Global Monitoring Division, National Oceanic and Atmospheric Administration (NOAA), U.S. Department of Commerce. 2015. Available from [http://www.esrl.noaa.gov/gmd/ccgg/trends/#mlo\\_full](http://www.esrl.noaa.gov/gmd/ccgg/trends/#mlo_full). [Access online 24 September 2015].
4. Freund, H. J. and Roberts, M. W. (1996). Surface chemistry of carbon dioxide. *Surface Science Reports*, 25: 225 – 273.
5. Son, W. J., Choi, J. S. and Ahn, W. S. (2008) Adsorptive removal of carbon dioxide using polyethyleneimine-loaded mesoporous silica materials. *Microporous and Mesoporous Materials*, 113: 31 – 40.
6. Abanades, J. C. (2002). The maximum capture efficiency of CO<sub>2</sub> using a carbonation/ calcination cycle of CaO/CaCO<sub>3</sub>, *Chemical Engineering Journal*, 90: 303 – 306.

7. Kwon, J. H., Dai, M., Halls, M. D., Langereis, E., Chabal, Y. J. and Gordon, R. G. (2009). In situ infrared characterization during atomic layer deposition of lanthanum oxide. *Journal of Physical Chemistry C.*, 113: 654 – 660.
8. Rosynek, M. P. and Magnuson, D. T. (1977). Infrared study of CO<sub>2</sub> adsorption on lanthanum sesquioxide and trihydroxide. *Journal of Catalysis*, 48: 417 – 421.
9. Okawa, Y. and Tanaka, K. (1995). STM investigation of the reaction of Ag-O added rows with CO<sub>2</sub> on a Ag (110) surface. *Surface Science*, 344: 1207 – 1212.
10. Yoshikawa, K., Sato, H., Kaneeda, M. and Kondo, J. M. (2014). Synthesis and analysis of CO<sub>2</sub> adsorbents based on cerium oxide. *Journal of CO<sub>2</sub> Utilization*, 8: 34 – 38.
11. Wan Isahak, W. N. R., Che Ramli, Z. A., Ismail, M. W., Ismail, K., Yusop, R. M., Mohamed Hisham, M. W. and Yarmo, M. A. (2013). Adsorption–desorption of CO<sub>2</sub> on different type of copper oxides surfaces: Physical and chemical attractions studies. *Journal of CO<sub>2</sub> Utilization*, 2: 8 – 15.
12. Hakim, A., Wan Isahak, W. N. R., Abu Tahari, M. N., Yusop, M. R., Mohamed Hisham, M. W., and Yarmo, M. A. (2014). Temperature programmed desorption of carbon dioxide for activated carbon supported nickel oxide: The adsorption and desorption studies. *Advanced Materials Research*, 1087: 45 – 49.
13. Seyller, T., Borgmann, D. and Wedler, G. (1998). Interaction of CO<sub>2</sub> with Cs-promoted Fe (110) as compared to Fe (110) /K + CO<sub>2</sub>. *Surface Science*, 400: 63 – 79.
14. Ramis, G., Busca, G. and Lorenzelli, V. (1991). Low-temperature CO<sub>2</sub> adsorption on metal oxides: Spectroscopic characterization of some weakly adsorbed species. *Materials Chemistry and Physics*, 29: 425 – 435.
15. Ferretto, L. and Glisenti, A. (2002). Study of the surface acidity of an hematite powder. *Journal of Molecular Catalysis A: Chemical*, 187: 119 – 128.
16. Lefevre, G. (2004). In situ Fourier-transform infrared spectroscopy studies of inorganic ions adsorption on metal oxides and hydroxides. *Advance in Colloid and Interface Science*, 107: 109 – 123.
17. Baltrusaitis, J., Schuttlefield, J., Zeitler, E. and Grassian, V. H. (2011). Carbon dioxide adsorption on oxide nanoparticle surfaces. *Chemical Engineering Journal*, 170: 471 – 481.
18. Ismail, H. M., Cadenhead D. A. and Zaki, M. I. (1997). Surface reactivity of iron oxide pigmentary powders toward atmospheric components: XPS, FESEM, and gravimetry of CO and CO<sub>2</sub> adsorption. *Journal of Colloid and Interface Science*, 194: 482 – 488.
19. Dong, W. T., Wu, S. X., Chen, D. P., Jiang, X. W. and Zhu, C. S. (2000). Preparation of  $\alpha$ -Fe<sub>2</sub>O<sub>3</sub> nanoparticles by sol-gel process with inorganic iron salt. *Chemistry Letters*, 496 – 497.
20. Condon, J. B. (2006). *Surface area and porosity determinations by physisorption measurements and theory*, 1<sup>st</sup> ed., Elsevier, UK: pp. 1 – 28.
21. Hu, Z. H., Srinivasan, M. P. and Ni, Y. M. (2001). Novel activation process for preparing highly microporous and mesoporous activated carbons. *Carbon*, 39: 877 – 886.
22. Puziy, A. M., Poddubnaya, O. I., Martinez-Alonso, A., Suarez-Garcia, F. and Tascon, J. M. D. (2002). Synthetic carbons activated with phosphoric acid II. Porous structure. *Carbon*, 40: 1507 – 1519.
23. Kennedy, L. J., Mohan das, K. and Sekaran, G. (2004). Integrated biological and catalytic oxidation of organics/ inorganics in tannery wastewater by rice husk based mesoporous activated carbon-Bacillus sp. *Carbon*, 42: 2399 – 2407.
24. Sing, K. S. W., Everett, D. H., Haul, R. A. W., Moscou, L., Pierotti, R. A., Rouquerol, J. and Siemieniowska, T. (1985). Reporting physisorption data for gas/solid systems with special reference to the determination of surface area and porosity. *International Union of Pure and Applied Chemistry*, 57 (4): 603 – 619.
25. Gauden, O. A., Terzyk, A. P., Jaroniec, M. and Kowalczyk, P. (2007). Bimodal pore size distributions for carbons: Experimental results and computational studies. *Journal of Colloid and Interface Science*, 310: 205 – 216.
26. Choudhary, V. R., Mulla, S. A. R. and Uphade, B. S. (1999). Oxidative coupling of methane over alkaline earth oxides deposited on commercial support pre-coated with rare earth oxides. *Fuel*, 78: 427 – 437.
27. Kus, S., Otremba, M., Torz, A. and Taniewski, M. (2002). Further evidence of responsibility of impurities in MgO for variability in its basicity and catalytic performance in oxidative coupling of methane. *Fuel*, 81: 1755 – 1760.
28. Di Cosimo, J. I., Diez, V. K., Xu, M., Iglesia, E. and Apesteguia, C. R. (1998). Structure and surface and catalytic properties of Mg-Al basic oxides. *Journal of Catalysis*, 178: 499 – 510.

29. Su, C. M. and Suarez, D. L. (1997). In situ infrared speciation of adsorbed carbonate on aluminium and iron oxides. *Clays and Clay Mineral*, 45(6): 814 – 825.
30. Rebenstorf, B. (1991). Modified chromium/silica gel catalysts: An FTIR study of the addition of alkali metal ions. *Acta Chemica Scandinavica*, 45: 1012 – 1017.
31. Belskaya, O. B., Danilova, I. G., Kazakov, M. O., Mironenko, R. M., Lavrenov, A. V. and Likholobov, V. A. (2012). FTIR spectroscopy of adsorbed probe molecules for analyzing the surface properties of supported Pt (Pd) Catalysts, In T. Theophile (Ed.). *Infrared Spectroscopy - Materials Science, Engineering and Technology*, In Tech., Croatia: pp. 149 – 178
32. Chauhan, S. M. and Chakrabarty, B. S. (2014). Lead (Pb) doped fluoride nanocrystals: structural and optical properties. *International Journal of Advanced Research*, 2 (7): 607 – 614.
33. Bishop, J. L., Murad, E., Madejova, J., Komadel, P., Wagner, U. and Scheinost, A. C. (1999). Visible, Mossbauer and infrared spectroscopy of dioctahedral smectites: Structural analyses of the Fe-bearing smectites Sampor, SWy-1 and SWa-1: *11<sup>th</sup> International Clay Conference*, Ottawa: pp. 413 – 419.
34. Taylor, R. M. (1980). Formation and properties of Fe (II) Fe (III) hydroxyl-carbonate and its possible significance in soil formation. *Clay Mineral*, 15: 369 – 382.